LAWRENCE
LIVERMORE
NATIONAL
LABORATORY

LLNL-JRNL-578336

Characterization of Blistering and Delamination in Depleted Uranium Hohlraums

K. J. M. Blobaum, M. Stadermann, J. Fair, N. Teslich, M. Wall, R. Foreman, N. Hein, H. Streckert, A. Nikroo

August 31, 2012

Fusion Science and Technology

Disclaimer

This document was prepared as an account of work sponsored by an agency of the United States government. Neither the United States government nor Lawrence Livermore National Security, LLC, nor any of their employees makes any warranty, expressed or implied, or assumes any legal liability or responsibility for the accuracy, completeness, or usefulness of any information, apparatus, product, or process disclosed, or represents that its use would not infringe privately owned rights. Reference herein to any specific commercial product, process, or service by trade name, trademark, manufacturer, or otherwise does not necessarily constitute or imply its endorsement, recommendation, or favoring by the United States government or Lawrence Livermore National Security, LLC. The views and opinions of authors expressed herein do not necessarily state or reflect those of the United States government or Lawrence Livermore National Security, LLC, and shall not be used for advertising or product endorsement purposes.

Characterization of Blistering and Delamination in Depleted Uranium Hohlraums

Kerri J.M. Blobaum, Lawrence Livermore National Laboratory
Michael Stadermann, Lawrence Livermore National Laboratory
James E. Fair, Lawrence Livermore National Laboratory
Nick E. Teslich, Jr., Lawrence Livermore National Laboratory
Mark A. Wall, Lawrence Livermore National Laboratory
Ronald J. Foreman, Lawrence Livermore National Laboratory
Nick Hein, General Atomics
Hal Streckert, General Atomics
Abbas Nikroo, General Atomics

Contact Author:
Kerri Blobaum
Lawrence Livermore National Laboratory
L-356, 7000 East Avenue
Livermore, CA 94550
(925) 422-3289 (phone)
blobaum1@llnl.gov

Total number of pages: 34
Number of tables: 1
Number of figures: 13
No color figures

CHARACTERIZATION OF BLISTERING AND DELAMINATION IN DEPLETED URANIUM HOHLRAUMS

K.J.M. BLOBAUM,[a] M. STADERMANN, [a] J.E. FAIR, [a] N.E. TESLICH, [a] M.A. WALL, [a] R.J. FOREMAN, [a] N. HEIN, [b] H. STRECKERT, [b] A. NIKROO [b]

[a]*Lawrence Livermore National Laboratory, Livermore, California*
[b]*General Atomics, San Diego, California*

KEYWORDS: HOHLRAUM, DEPLETED URANIUM, BLISTER, SPUTTER DEPOSITION

ABSTRACT

Blistering and delamination are the primary failure mechanisms during the processing of depleted uranium (DU) hohlraums. These hohlraums consist of a sputter-deposited DU layer sandwiched between two sputter-deposited layers of gold; a final thick gold layer is electrodeposited on the exterior. The hohlraum is deposited on a copper-coated aluminum mandrel; the Al and Cu are removed with chemical etching after the gold and DU layers are deposited. After the mandrel is removed, blistering and delamination are observed on the interiors of some hohlraums, particularly at the radius region. It is hypothesized that blisters are caused by pinholes in the copper and gold layers; etchant leaking through these holes reaches the DU layer and causes it to oxidize, resulting in a blister. Depending on the residual stress in the deposited layers, blistering can initiate larger-scale delamination at layer interfaces. Scanning electron microscopy (SEM) indicates that inhomogeneities in the machined aluminum mandrel are replicated in the sputter-deposited copper layer. Furthermore, the Cu layer exhibits columnar growth with pinholes that likely allow etchant to come in contact with the gold layer. Any inhomogeneities or pinholes in this initial gold layer then become nucleation sites for blistering. Using a focused-ion beam (FIB) system to etch through the gold layer and extract a cross-sectional

sample for transmission electron microscopy (TEM), amorphous, intermixed layers at the gold/DU interfaces are observed. Nanometer-sized bubbles in the sputtered and electrodeposited gold layers are also present. Characterization of the morphology and composition of the deposited layers is the first step in determining modifications to processing parameters, with the goal of attaining a significant improvement in hohlraum yield.

I. INTRODUCTION

Hohlraums fabricated from depleted uranium (DU) and Au are used for ignition shots at the National Ignition Facility because they are expected to have a significant increase in capsule performance over gold-only hohlraums. Recent shots with equivalent capsules and laser performance demonstrated that the DU hohlraum lead to an earlier bangtime and increased x ray and neutron yields, compared to gold.[1] Currently, DU hohlraums are fabricated by sputter deposition; both surfaces of the uranium layer are covered with gold to protect them from oxidation and to provide structural stability. The fabrication process involves depositing the DU and Au layers on an aluminum mandrel, which is later chemically etched to leave the freestanding DU/Au structure. After the etching process, blistering and delamination are observed on approximately 30% of the parts, resulting in a significant reduction in hohlraum production yield. To reduce or eliminate this problem, it is essential to determine the root cause of the blistering, including identifying where the blistering originates. Here, we describe our efforts to characterize these defects and the microstructure of the hohlraums using a combination of optical microscopy, scanning electron microscopy (SEM), and transmission electron microscopy (TEM). Our preliminary work indicates that the chemical etchants attack the DU, resulting in oxidation and delamination at the inner DU/Au interface, which results in macroscopic blisters.

The DU hohlraums are fabricated in two parts, which are assembled later. A schematic diagram of one of these parts is shown in Figure 1. An aluminum mandrel (1100 alloy) is machined using a diamond turning lathe; the mandrel includes various machined features that are replicated in the subsequently deposited layers. The Al mandrel is ion etched to improve adhesion and then coated with a ~0.2 μm thick sputter-deposited copper layer.

The purpose of the Cu layer is to protect the Au and DU layers during the harsh NaOH etch used to dissolve the Al mandrel at the end of the fabrication process. A ~0.7 μm thick layer of Au is deposited on top of the Cu. Again, this is a protective layer designed to prevent oxidation and corrosion of the DU. The subsequent ~10 μm thick DU layer is sputtered in the same chamber as the Au and it is capped with another ~0.7 μm thick sputtered Au layer. The parts are then removed from the sputtering chamber and coated with 20 μm of electrodeposited Au. This layer provides structure for the hohlraum and does not participate in ignition experiments. Hohlraums are back-machined and milled to produce the final exterior features, and then the Al mandrel and Cu layers are chemically removed. It is at this point in the fabrication process where blisters on the interior of the hohlraum can finally be observed.

The majority of blisters form on the hohlraum "radius," which is the curved region where the cylindrical barrel transitions to the flat laser entrance hole (LEH) end (see Figure 1). Given the geometry of this region, it is expected that the stress state of sputtered films is different here than along the barrel, or at the LEH. Residual stress in the deposited layers likely plays a role in enhanced blister formation at the radius. Examples of blisters at the radius are shown in Figure 2.

II. AS-DEPOSITED MICROSTRUCTURE

The first step in determining the cause of blistering is microstructural characterization of the as-deposited layers, particularly at the interfaces, which are likely planes for delamination. Using a FIB, we cut trenches into the hohlraum layers, allowing a cross-sectional view of the microstructure and interfaces with the incorporated SEM and

energy-dispersive spectroscopy (EDS) capabilities. The FIB can also be used to extract samples for TEM, where finer features can be identified.

II.A. Interfaces

Figure 3 shows TEM images of a FIB liftout from an as-deposited DU hohlraum that was still on the Al mandrel and had not been exposed to a chemical etch. The liftout was extracted perpendicular to the cylinder surface so that the interfaces between the Au and DU layers could be examined in cross section. Intermixed, amorphous Au/DU layers are observed at both Au/DU interfaces. The amorphous layer between the Au liner and the DU is 100 ± 5 nm thick and the layer between the DU and outer Au is 40 ± 5 nm thick. Compositional analysis of the layer at the Au liner/DU interface indicates that the composition varies nearly linearly.

This amorphous intermixed layer could form and/or grow via three mechanisms, which are not necessarily independent. First, mixing occurs as the impinging atoms bombard the surface with high energy and embed in, or displace, the already-deposited material.[2] The sputter-deposition process used to fabricate these hohlraums involves a negative bias on the substrate, which accelerates the sputtered atoms toward the substrate, increasing their kinetic energy. When these high-energy, high-mass U and Au atoms impinge on the substrate, the impact can induce atomic exchange, where the adatom penetrates the surface and an atom from the underlying lattice is ejected the top of the film.[3] This can result in an intermixed interface layer. Second, argon ions which are used to sputter material from the targets are also accelerated toward the biased substrate where they can enhance mixing and become incorporated into the growing film.[4] Third, the high

energy of the impinging atoms heats the substrate, enhancing surface mobility and atomic diffusion. Thus, an amorphous intermixed layer could form via a solid-state amorphization reaction (SSAR), where atomic diffusion occurs across the interface;[5, 6] this layer can continue to thicken throughout the course of the sputter deposition as the hohlraum remains at an elevated temperature.

Because the amorphous layers formed during the deposition of DU hohlraums are considerably thicker than what would be expected from intermixing during deposition alone (~5 nm)[7], they most likely grow via a SSAR. Furthermore, the amorphous layer between the Au liner and the DU layer is 100 nm thick and the layer between the DU layer and the outer Au layer is 40 nm thick. The former experiences more time at elevated temperature while the DU and subsequent layers are sputtered, and thus it has more time to grow, indicating that a time-dependent process, such as diffusion, is involved. Amorphous layers formed by solid-state reactions are found at the interfaces of many multilayered metallic composites.[8-11] Amorphization can even occur in immiscible systems, such as U and Au.[12] The temperature required for such amorphous phase formation is quite low, on the order of 150 - 300°C;[8, 13] the slightly elevated temperatures experienced by substrates during sputter deposition can be sufficient for SSARs to occur.[14, 15]

Assuming that diffusion is responsible for the formation of the amorphous, intermixed layers, the thicknesses of these layers can be used to calculate the deposition temperature. Each Au/DU interface in the hohlraum can be treated like a diffusion couple composed of two adjacent semi-infinite slabs (sputtered Au and DU). The solution to Fick's laws for this condition is given in equation 1 (variables are defined in Table 1):

$$C_x = \left(\frac{C_1+C_2}{2}\right) - \left(\frac{C_1-C_2}{2}\right) erf\left(\frac{x}{2\sqrt{Dt}}\right) \quad (1)$$

Calculation of the deposition temperature requires 3 assumptions: 1) the amorphous layer is formed *only* by interdiffusion of U and Au (*i.e.*, no mechanical intermixing occurs during sputtering); 2) The width of the intermixed layer is defined by what is measured in the TEM micrograph based on changes in contrast, and the measureable change in contrast corresponds to 1% concentration change; 3) The diffusion coefficients for Au in U and U in Au are equal (*D* for Au in U is available in the literature[16], but *D* for U in Au has not been measured). Based on these assumptions, the sputter-deposition temperature is calculated to be 214 ± 13°C based on the thickness of the Au liner/DU interfacial layer (100 nm); using the thickness of the outer Au/DU interfacial layer (40 nm), the deposition temperature is calculated to be 232 ± 13°C. Thus, the average deposition temperature is 222 ± 18°C. Within the uncertainty, the temperatures calculated from the thicknesses of the two amorphous layers are the same. This suggests that a thermally activated solid-state diffusional reaction is primarily responsible for the formation of the amorphous layer.

Adhesion between the DU and Au layers is probably improved by the interfacial intermixed layer. Furthermore, no oxidation of the DU was observed in the region with a coherent amorphous intermixed layer. Oxidation of the DU due to gettering of any residual oxygen or water in the sputter chamber is of particular concern because it would likely lead to blistering and delamination. SEM imaging showed delamination along the DU/Au interface in some regions, and these areas are currently being investigated further.

II.B. Grain Size and Morphology

The grain size of the DU is unexpectedly large for a sputter-deposited film. While it is difficult to obtain an accurate grain size measurement as the grains extend beyond the field of view of the TEM micrographs, we estimate the grain size to be on the order of several microns (Figure 3b). The morphology of these grains does not appear to be columnar. The elevated deposition temperature (222 ± 18°C) may be sufficient to permit large, equiaxed grains to grow during deposition.

The sputter-deposited Au layers have a columnar morphology, with the height of the columns typically extending across the thickness of the layer (~0.7 μm). The lateral (in-plane) dimension is 0.18 ± 0.05 μm. Twins are present in some of the grains.

II.C. Incorporated Bubbles and Voids

TEM images of as-deposited hohlraums (i.e., prior to chemical etching) reveal the presence of nanometer-scale bubbles and/or voids in some of the hohlraum layers, with higher concentrations found at, or near, the interfaces. These features are too small to be observed with SEM, and can only be seen in the TEM using the Fresnel imaging technique with under- or over-focus conditions.[17] Round features with diameters on the order of a few nanometers or less are typically called "bubbles." Bubbles are gas-filled, and they nucleate when occupied vacancies migrate and coalesce. The driving force for bubble formation is the decrease in energy resulting from the formation of a di-vacancy or elimination of a vacancy, and the size is limited by a combination of factors including strength of the metal matrix, internal gas pressure, and surface energy.[18] Voids, on the other hand, result from migration and coalescence of vacancies and other defects, and they are not gas-filled. Typically, voids are larger than bubbles and their perimeters are faceted.

Because the hohlraum layers are fabricated by sputter-deposition and electrodeposition, it is likely that the nanometer-sized features are gas-filled bubbles, rather than voids. Bubbles formed by incorporation of sputter gas or residual gases in the deposition chamber have been reported in sputter-deposited and evaporated films. [19-22] Electrodeposited films can also contain bubbles formed by hydrogen or oxygen evolution during the aqueous deposition process.[23]

At the Au liner/Cu interface, there are small bubbles (diameter ~ 2 nm) in the gold layer and larger bubbles (~10 nm) extending from the interface into the Cu layer (Figure 4). In the Au layer, the bubbles are primarily located near the Au/Cu interface, with their number density decreasing sharply as the distance from the interface increases. These bubbles are likely filled with argon sputter gas, which is incorporated during deposition. It is possible that the elevated temperatures during deposition allowed bubbles to migrate toward the lower energy Au/Cu interface, where they coalesced on the grain boundaries. Another reason for the enhanced bubble density at the interface may be the roughness of the ion-milled Cu surface, which allows more Ar to adsorb and become trapped as Au islands form and grow together.[21]

A similar pattern of large bubbles at the interface and smaller bubbles in the bulk is seen at the interface between the outer layer of sputtered Au and the electrodeposited Au (Figure 5a). Here, large bubbles (20 – 30 nm) are concentrated in the electrodeposited Au near, but not at, the interface. In the bulk of the electrodeposited Au, small (~2 nm) bubbles are uniformly distributed through the thickness (Figure 5b). These bubbles likely contain hydrogen that was evolved from the hydrolysis of water in the aqueous deposition bath. The current used during the deposition is sufficiently high for this process to occur.

III. INTERFACIAL DELAMINATION AND BLISTERING

The preceding characterization of the Au/DU hohlraum microstructure was performed on an as-deposited sample, prior to any chemical etching. Blistering prior to etching is rare, and it is hypothesized that the chemical etch to remove the Al mandrel and Cu layer attacks the DU and causes blistering and delamination.

To test this hypothesis, we used the FIB to ion mill into a blister found on a hohlraum that had gone through all production steps. By peering into the trench with the SEM and using EDS, it was possible to determine that delamination occurred between the Au liner and the DU layer (Figure 6). For comparison, a nearby unblistered region on the same hohlraum sample was also ion milled to investigate the Au liner/DU interface, and a sample was extracted for TEM analysis. In this sample, pitting at the Au liner/DU interface was observed, even though the exterior Au liner surface appeared pristine (Figure 7). Pinholes in the Au liner, as well as delamination propagating along the interface are also seen. Electron diffraction in the TEM indicates nanocrystalline and amorphous regions that are likely to be uranium oxides or hydrides. Pitting and corrosion were not observed in the as-deposited microstructure and therefore we conclude that the chemical etch is responsible for this degradation and delamination.

III.A. Permeability of Cu and Au Protective Layers

The purposes of the Cu layer and Au liner are primarily to protect the DU during etching. However, the blistering and corrosion observed at the Au liner/DU interface indicate that etchant is permeating both of these layers and attacking the DU. To test the

effectiveness of these two layers, a sample containing only the Cu and Au liner layers sputtered on an Al mandrel was subjected to a harsh nitric acid etch (more severe than the etching conditions used for hohlraum production). Nitric acid etches Cu, so if the Au liner layer is permeable, we would expect to see degradation of the Cu. After this etch, the surface of the sample was peppered with ~50 μm diameter blisters (Figure 8a). Some of these blisters were cracked (Figure 8b), and others had Al_2O_3 at their apogees (Figure 8c). FIB cross-sections through blisters showed that much of the Cu layer had dissolved and was replaced by a layer of Al_2O_3 that had grown from the Al mandrel (Figure 8d). The Cu layer had been reduced from a continuous layer to randomly spaced hillocks surrounded by Al_2O_3.

To determine why the Au liner and Cu layer are permeable, SEM was employed to search for evidence of pinholes. While through-holes were not specifically identified in these layers, the rough microstructure suggests that there are permeation paths. Rough substrates are reported to lead to a higher number of pinholes.[24] Beginning with the Au liner, the roughness and asperities were traced back to the Al mandrel surface, which is replicated through the sputtered Cu and Au liner layers.

SEM images of the Au liner microstructure in plan view are shown in Figure 9. The microstructure is columnar, with strings of asperities that run parallel to the long axis of the hohlraum. The Cu layer shows a similar microstructure, with asperity strings and faceted islands (Figure 10). The surface of the Cu appears porous; the columnar grains have not fully grown together, leaving voids between the grains (Figure 11). Images of the machined Al mandrel also show a rough microstructure, with strings of impurities running along the length of the mandrel, which is the extrusion direction for the Al rod used as the starting

material. The 1100 Al alloy used here contains hard Si and Fe inclusions that can dull machining tools, resulting in the flaked surface shown in Figure 12a. After ion milling of the Al mandrel, the impurities are even more evident. The ion milling preferentially etches the Al, leaving behind strings of Fe and Si asperities (Figure 12b). These features are then replicated in all subsequent deposited layers, which can result in voids and paths for chemical etchants to permeate the layers.

IV. PROCESS IMPROVEMENTS

Permeation of the chemical etchants appears to be a key factor in blister formation. Therefore, steps that improve the quality of the protective Cu and Au liner layers are key to increasing hohlraum production yield.

Because asperities in the Cu and Au liner layers appear to originate on the Al mandrel, improving this surface may improve the yield. One way to improve the surface is the use a cleaner Al substrate, rather than an alloy with known inclusions. SEM images of Al mandrels machined from 99.99% Al are shown in Figure 13. The parallel lines on these images are the tool marks; the asperities and flaking of the surface that are seen in the Al 1100 alloy mandrels are not present here. Additionally, a shorter ion etch time may improve the Al surface because the inclusions will not become as pronounced when the Al is preferentially removed. However, decreasing the ion etch time may result in poor Cu adhesion. Recent limited-quantity trials with Al mandrels that were etched for half the time normally used produced excellent quality hohlraums. More trials are needed to verify that shorter ion etch times increase the yield on a production-quantity scale.

Another method for decreasing etchant permeation is to increase the number of protective layers. This decreases the likelihood that a pinhole through any given layer will be coincident with the layer above or below it.[24] Currently, work is underway to add an additional electrodeposited Cu layer to the sputter-deposited Cu layer. Adhesion of additional layers, however, can be an issue.

Modifying the geometry of the Al mandrel may also decrease blistering. If some of the Al is physically removed prior to the chemical etch (*e.g.*, by boring material from the center of the mandrel), the etch time can be decreased. This method is also currently under investigation.

V. CONCLUSIONS

Characterization of Au/DU hohlraums at various stages of production indicates that blistering is primarily the result of delamination between the Au liner and the DU layer. Wet chemical etchants used to dissolve the Al mandrel and Cu layer seep through the Cu and Au liner, causing corrosion of the DU and delamination from the Au. Improving the protective Cu and Au liner layers, beginning with decreasing the roughness of the Al mandrel is likely to improve the production yield of these hohlraums.

Prepared by LLNL under Contract DE-AC52-07NA27344.

REFERENCES

1. D.A. CALLAHAN, N.B. MEEZAN, et al., "The velocity campaign for ignition on nif," *Phys. Plasmas*, **19,** 056305 (2012).

2. X.W. ZHOU, H.N.G. WADLEY, et al., "Atomic scale structure of sputtered metal multilayers," *Acta Mater.*, **49,** 4005 (2001).

3. X.W. ZHOU and H.N.G. WADLEY, "The low energy ion assisted control of interfacial structure: Ion incident energy effects," *J. Appl. Phys.*, **87,** 8487 (2000).

4. X.W. ZHOU and H.N.G. WADLEY, "Mechanisms of inert gas impact induced interlayer mixing in metal multilayers grown by sputter deposition," *J. Appl. Phys.*, **90,** 3359 (2001).

5. W.L. JOHNSON, "Thermodynamic and kinetic aspects of the crystal to glass transformation in metallic materials," *Prog. Mater. Sci.*, **30,** 81 (1986).

6. K. SAMWER, "Amorphization in solid metallic systems," *Phys. Rep.*, **161,** 1 (1988).

7. L.J. CHEN, I.W. WU, et al., "Effects of backsputtering and amorphous-silicon capping layer on the formation of tisi2 in sputtered ti films on (001)si by rapid thermal annealing," *J. Appl. Phys.*, **63,** 2778 (1988).

8. S. SCHNEIDER, H. SCHRODER, et al., "Phase sequence in the solid-state amorphization reaction of metallic thin-films," *Thin Solid Films*, **174,** 11 (1989).

9. R.B. SCHWARZ and W.L. JOHNSON, "Formation of an amorphous alloy by solid-state reaction of the pure polycrystalline metals," *Phys. Rev. Lett.*, **51,** 415 (1983).

10. B.M. CLEMENS and T.C. HUFNAGEL, "Amorphous-alloys formed by solid-state reaction," *J. Alloy Compd.*, **194,** 221 (1993).

11. K. BARMAK, C. MICHAELSEN, and G. LUCADAMO, "Reactive phase formation in sputter-deposited ni/al multilayer thin films," *J. Mater. Res.*, **12,** 133 (1997).

12. C. MICHAELSEN, C. GENTE, and R. BORMANN, "The thermodynamics of amorphous phases in immiscible systems: The example of sputter-deposited nb-cu alloys," *J. Appl. Phys.*, **81,** 6024 (1997).

13. B. BLANPAIN, L.H. ALLEN, et al., "Solid-state amorphization in al-pt multilayers by low-temperature annealing," *Phys. Rev. B*, **39,** 13067 (1989).

14. R.J. HIGHMORE, R.E. SOMEKH, et al., "A differential scanning calorimetry study of solid-state amorphization in multilayer ni/zr," *Mater. Sci. Eng.*, **97,** 83 (1988).

15. T.C. HUFNAGEL, S. BRENNAN, et al., "Observation of a rapid amorphization reaction," *J. Mater. Res.*, **7,** 1976 (1992).

16. S.J. ROTHMAN, "The diffusion of gold in gamma-uranium," *J. Nucl. Mater.*, **3,** 77 (1961).

17. A.J. SCHWARTZ, M.A. WALL, et al., "Characterization and modelling of helium bubbles in self-irradiated plutonium alloys," *Philos. Mag.*, **85,** 479 (2005).

18. J.R. JEFFRIES, M.A. WALL, et al., "He bubble coarsening by migration and coalescence in annealed pu-ga alloys," *J. Nucl. Mater.*, **410,** 84 (2011).

19. R. ANDREW and V. KRASEVEC, "Grain coarsening and gas-bubbles in annealed gold-films," *Philos. Mag.*, **31,** 1295 (1975).

20. S. NAKAHARA, "Microporosity in thin-films," *Thin Solid Films*, **64,** 149 (1979).

21. S. NAKAHARA, "Microporosity induced by nucleation and growth processes in crystalline and non-crystalline films," *Thin Solid Films*, **45,** 421 (1977).

22. A. PRUYMBOOM, P. BERGHUIS, et al., "Argon bubbles in sputtered amorphous nb3ge films, studied by collective fluxpinning and transmission electron-microscopy," *IEEE T. Magn.*, **23,** 942 (1987).

23. Y. OKINAKA and S. NAKAHARA, "Structure of electroplated hard gold observed by transmission electron-microscopy," *J. Electrochem. Soc.*, **123,** 1284 (1976).

24. J. MUNEMASA and T. KUMAKIRI, "Effect of the surface roughness of substrates on the corrosion properties of films coated by physical vapour deposition," *Surf. Coat. Technol.*, **49,** 496 (1991).

Variable	Definition	Values used to calculate deposition temperature, T
C_x	Concentration at a distance x from the original interface	Au liner/DU: -50 < x < 50 nm Outer Au layer/DU: -20 < x < 20 nm 0.01 < C_x < 0.99
C_1	Initial concentration of uranium	1
C_2	Initial concentration of gold	0
D	Diffusion coefficient for Au in U[16]	$(4.86 \pm 1.3)\times 10^{-3} \cdot \exp((-30400 \pm 520)/RT)$ cm^2/sec
t	Time at temperature T	Au liner/DU: 5.8 hours Outer Au layer/DU: 0.3 hours
R	Universal gas constant	1.9859 cal/(K•mol)

Table 1

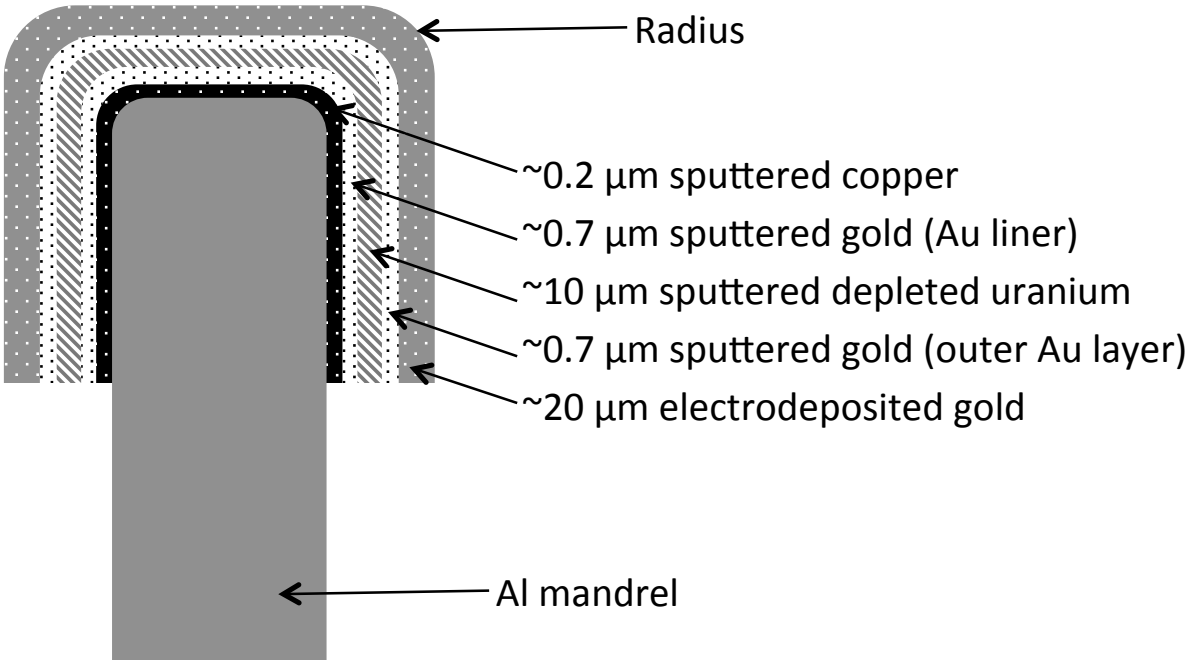
Radius
~0.2 µm sputtered copper
~0.7 µm sputtered gold (Au liner)
~10 µm sputtered depleted uranium
~0.7 µm sputtered gold (outer Au layer)
~20 µm electrodeposited gold
Al mandrel

Figure 1

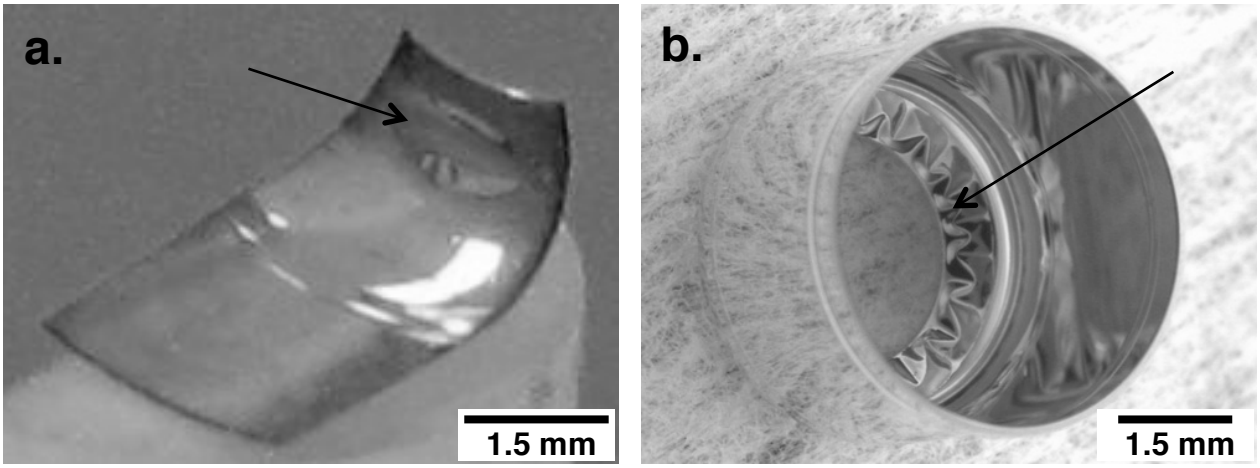

Figure 2

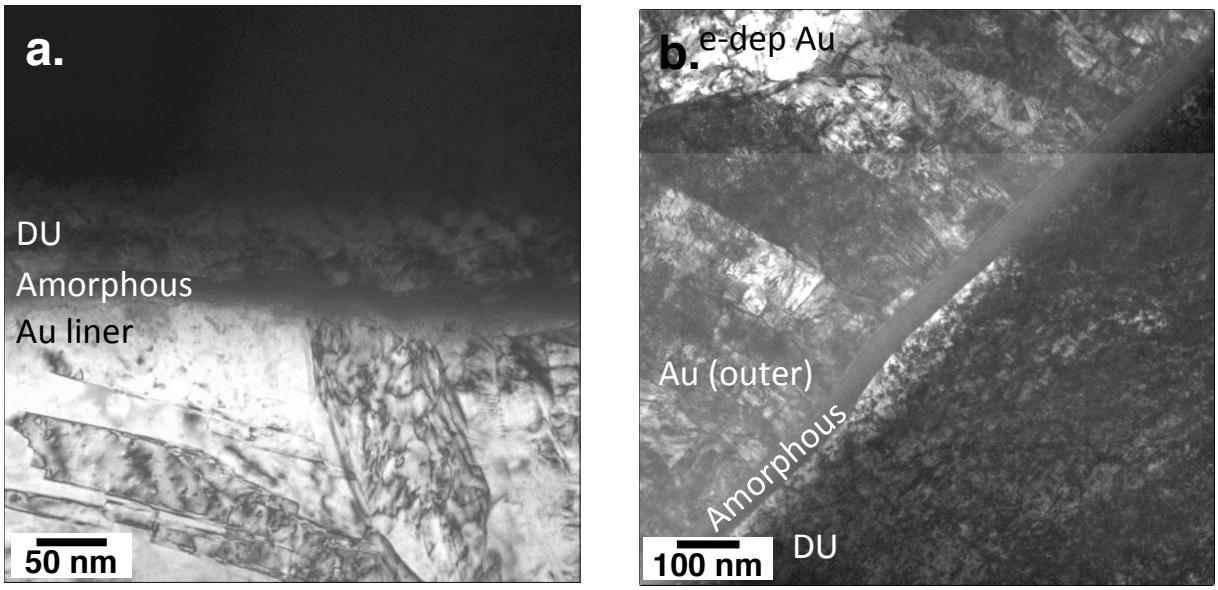
a.
DU
Amorphous
Au liner
50 nm
b.
e-dep Au
Au (outer)
Amorphous
DU
100 nm

Figure 3

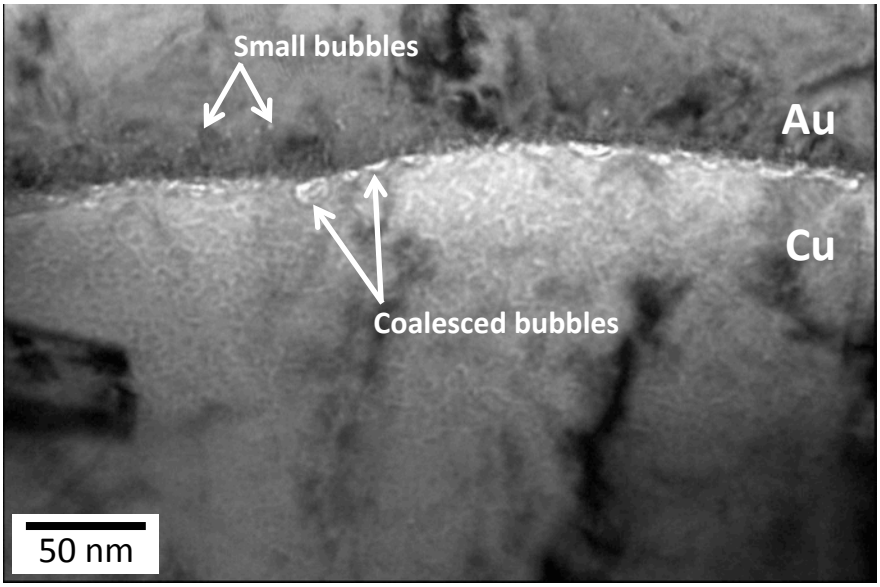

Figure 4

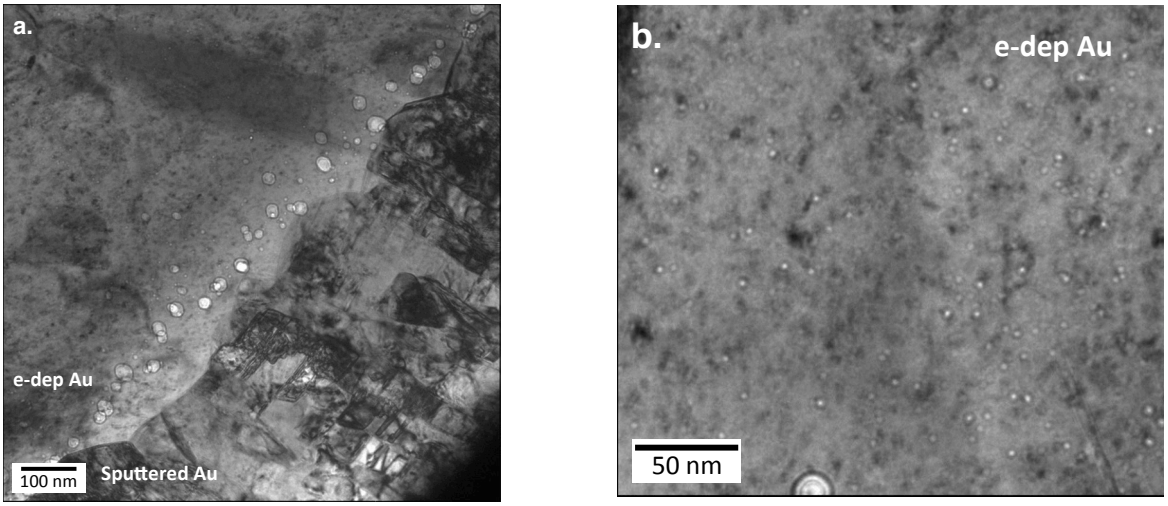

Figure 5

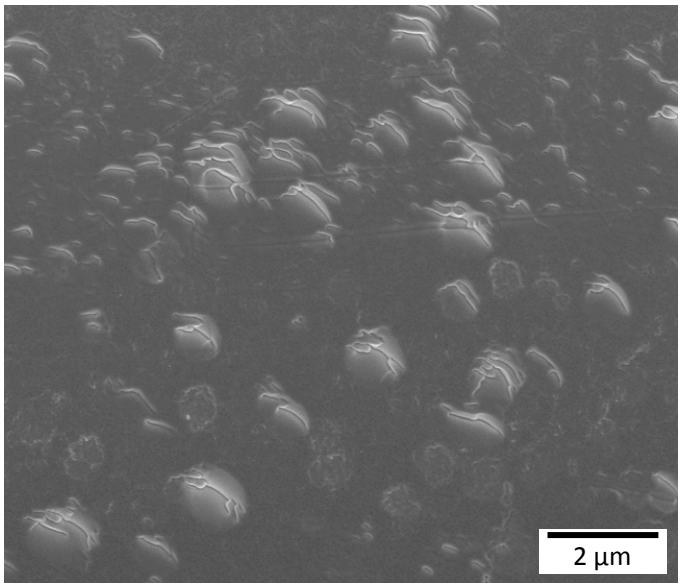

Figure 6

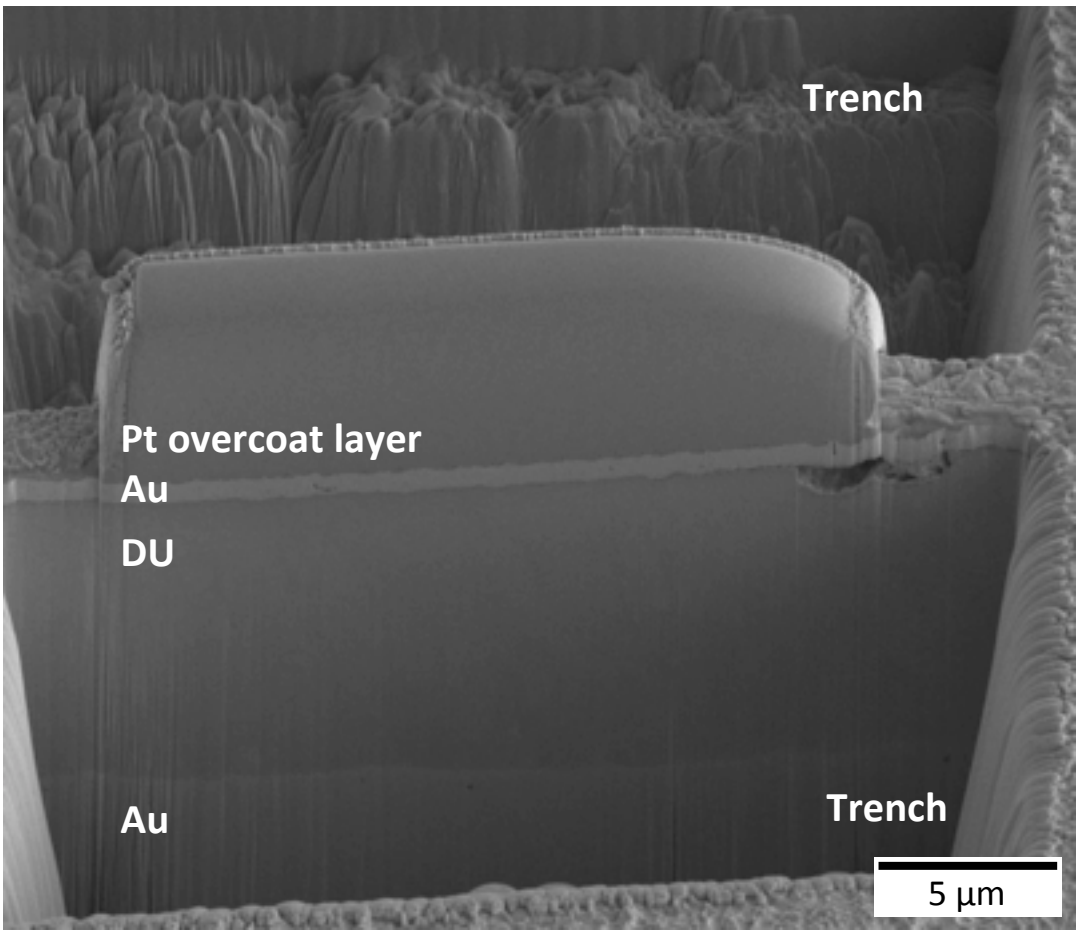

Figure 7

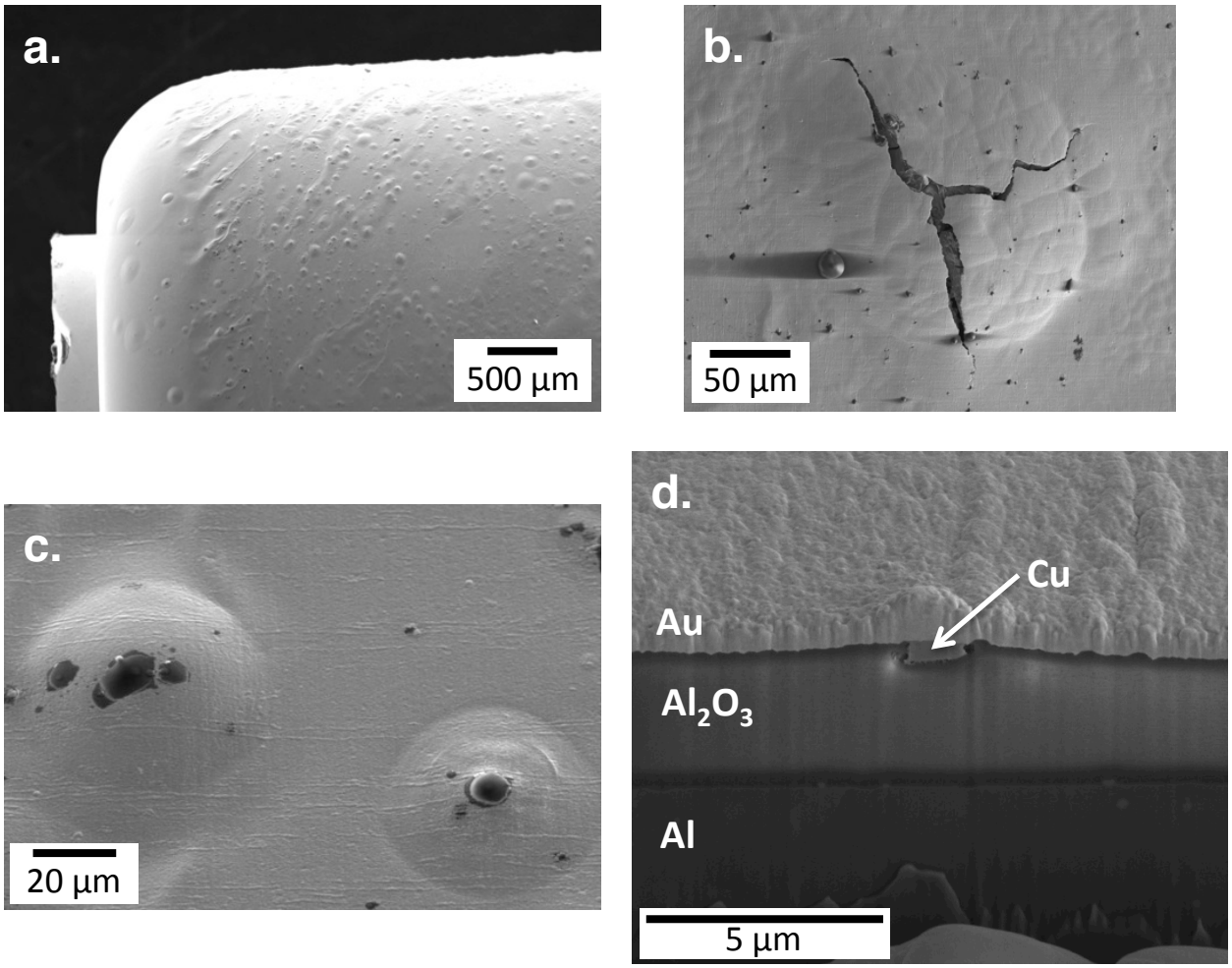

Figure 8

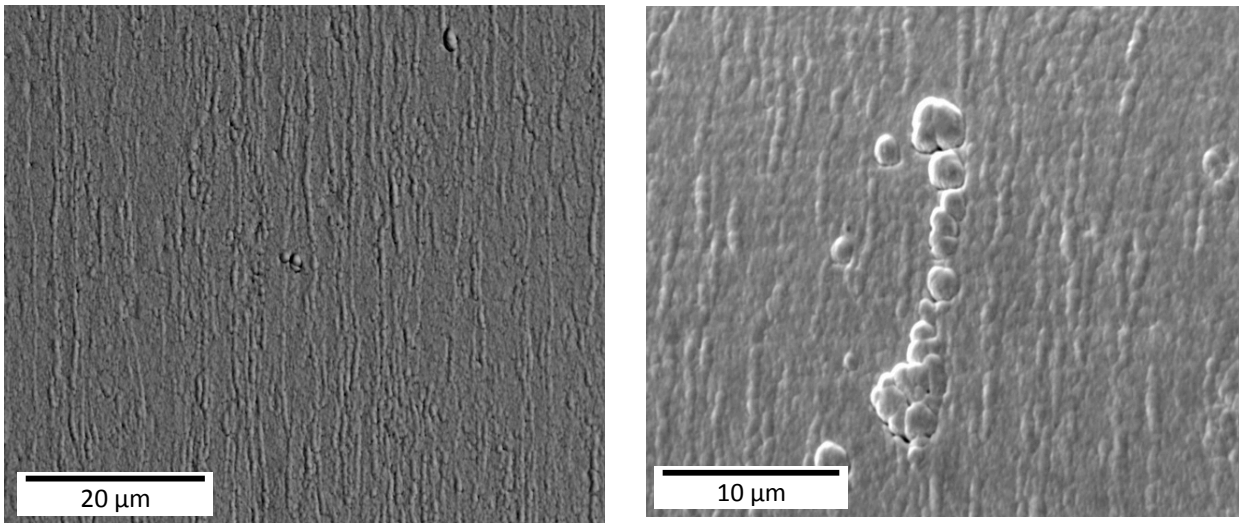

Figure 9

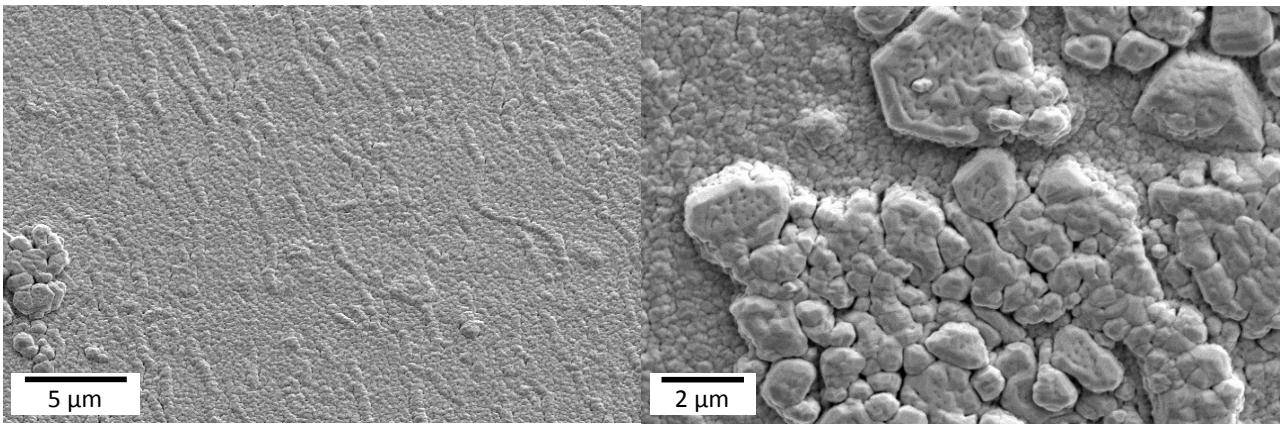

Figure 10

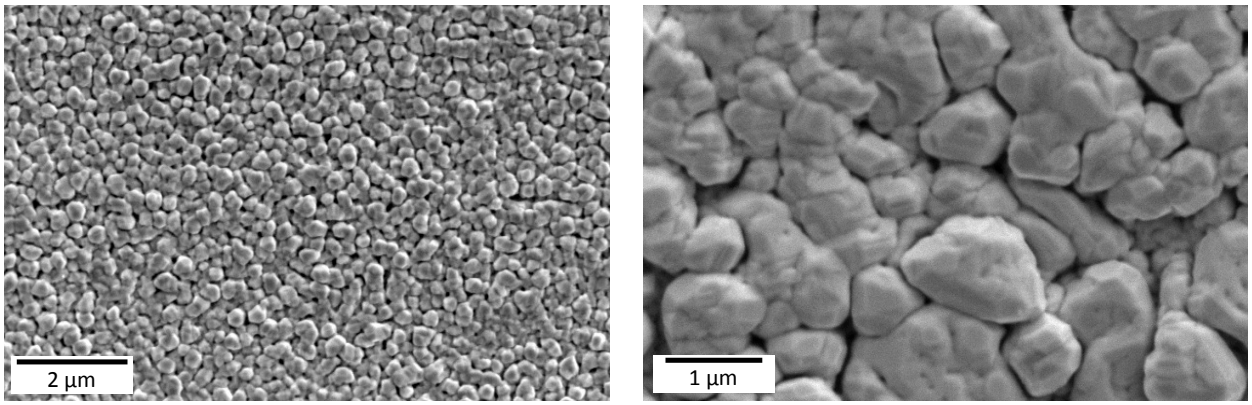

Figure 11

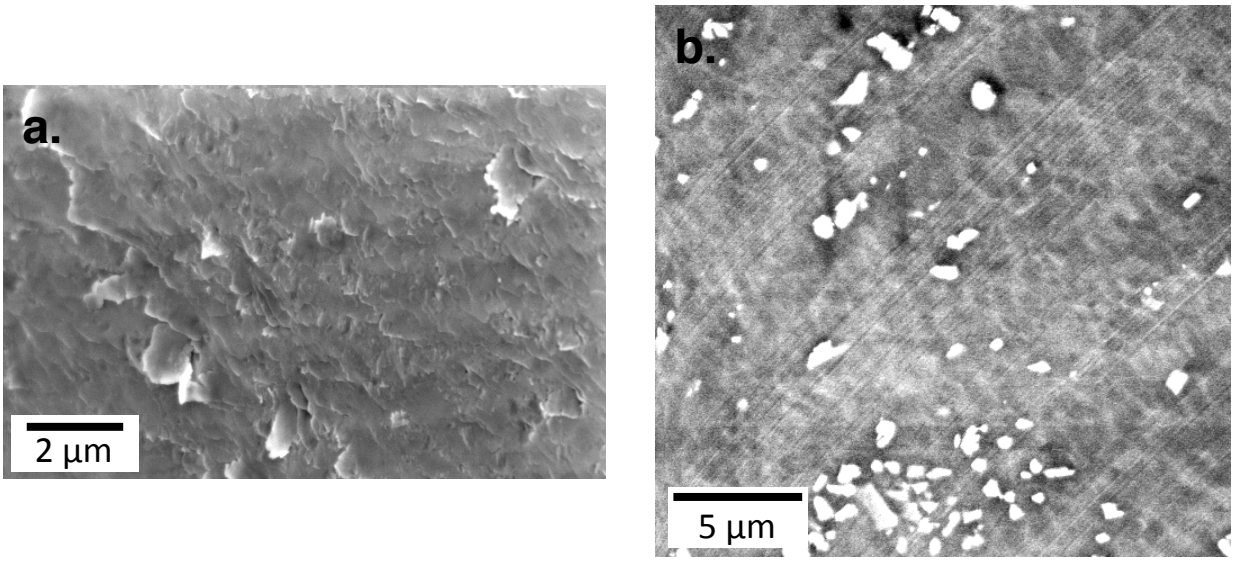

Figure 12

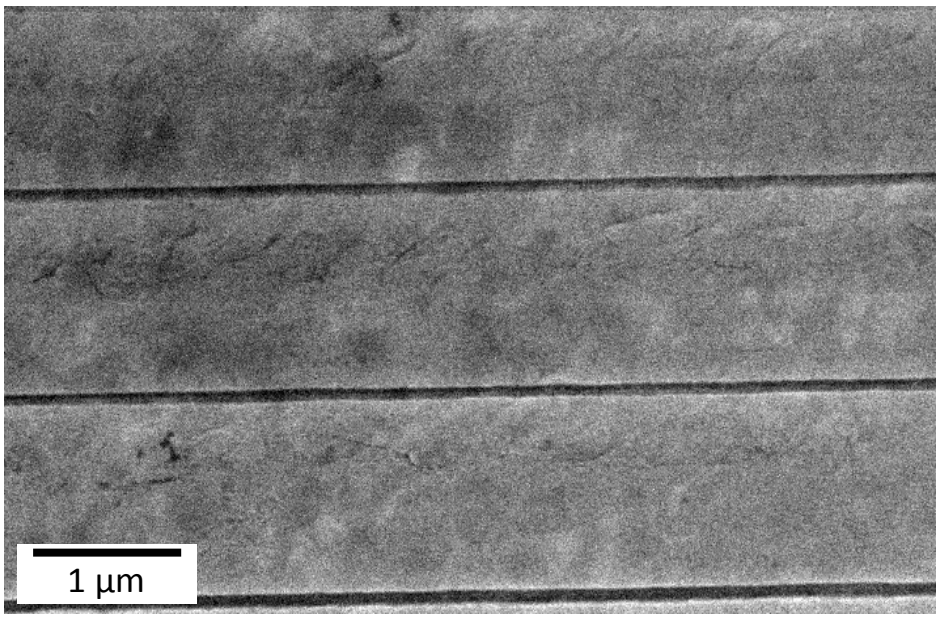

Figure 13

Table and Figure Captions

Table 1: Variables and values used in calculating deposition temperature using Fick's laws.

Figure 1: Schematic diagram showing the layers in a DU hohlraum (not to scale, and detailed features have been omitted). The Al mandrel and sputtered copper are chemically etched, leaving a freestanding hohlraum consisting of DU sandwiched between layers of gold.

Figure 2: Optical images of DU hohlraums showing blistering on the interior, at the radius. The blister shown in (a) is a single isolated blister, while the blistering in (b) is a rippled delamination that extends around the circumference of the hohlraum.

Figure 3: TEM images of the DU/Au interfaces in an as-deposited hohlraum. At the interface, there is an amorphous, intermixed layer. The amorphous layer between the Au liner and DU (a) is 100 ± 5 nm thick; the layer between the outer Au layer and DU is 40 ± 5 nm thick. In (b), columnar Au grains are evident in the sputtered layer; the beginning of the electrodeposited Au layer is visible in the upper left corner.

Figure 4: TEM image of the sputtered copper/sputtered gold liner interface. Small bubbles (white circles) are seen in the gold layer near the interface. At the interface, and extending into the copper layer, larger bubbles are present.

Figure 5: TEM images of bubbles in the electrodeposited Au layer. In a.), large bubbles near the interface between the electrodeposited gold and sputtered gold layers are evident. The black spots in the electrodeposited gold layer are FIB-induced damage. Image b.) shows bubbles (small white circles) distributed through the bulk of the electrodeposited gold layer.

Figure 6: Cracked and corroded DU at the bottom of a trench milled into a hohlraum blister. Analysis of the trenched area revealed that the blistered delamination occurred between the Au liner and the DU layer.

Figure 7: A sample extracted from a hohlraum using the FIB. At the Au liner surface (*i.e.*, the inner surface of the hohlraum), this sample appeared pristine. However, as this SEM image shows, there is pitting below the surface at the Au liner/DU interface. (Note: the Pt overcoat layer is applied in the FIB to protect the sample's surface during ion milling.)

Figure 8: SEM images of blisters in a gold layer that was sputter-deposited onto a Cu-coated Al mandrel. The Au/Cu/Al assembly was etched in nitric acid. (a.) Radius area of the gold surface showing severe blistering. (b.) A cracked blister on the gold surface. (c.) Two Al_2O_3-topped blisters on the gold surface. (d.) Cross-sectional image of the mandrel. The Cu layer, previously covering the Al mandrel, has been almost entirely dissolved and replaced by Al_2O_3.

Figure 9: SEM images of the as-deposited Au liner. The microstructure has strings of asperities running along the long axis of the cylinder.

Figure 10: SEM images of the as-deposited Cu layer, which is sputtered on the Al mandrel. Similar to the gold liner, the surface shows strings of asperities. Some of the islands are faceted.

Figure 11: High-resolution SEM images of the sputter-deposited copper surface. The grains are columnar, and have not fully grown together, likely leading to paths for chemical etchants to leach through this layer.

Figure 12: SEM images of a machined Al 1100 mandrel surface. (a.) The flaked surface finish of the as-machined mandrel is caused by hard Si and Fe inclusions in the alloy, which dull the diamond tool. (b.) After ion etching, the hard inclusions (light contrast) are more prominent because the etch preferentially attacks the Al, leaving behind the impurities. These asperities are replicated in all subsequently deposited layers.

Figure 13: SEM image of the machined surface of a 99.99% Al mandrel. The parallel lines are tool cutting marks. The inclusions and flaking observed on mandrels machined from an Al 1100 alloy are not seen in this high-purity material.